REPORT DOCUMENTATION PAGE

Form Approved
OMB No. 0704-0188

The public reporting burden for this collection of information is estimated to average 1 hour per response, including the time for reviewing instructions, searching existing data sources, gathering and maintaining the data needed, and completing and reviewing the collection of information. Send comments regarding this burden estimate or any other aspect of this collection of information, including suggestions for reducing the burden, to the Department of Defense, Executive Services and Communications Directorate (0704-0188). Respondents should be aware that notwithstanding any other provision of law, no person shall be subject to any penalty for failing to comply with a collection of information if it does not display a currently valid OMB control number.
PLEASE DO NOT RETURN YOUR FORM TO THE ABOVE ORGANIZATION.

1. REPORT DATE *(DD-MM-YYYY)*	2. REPORT TYPE	3. DATES COVERED *(From - To)*
15-16-2010	Final	September 2008-March 2010

4. TITLE AND SUBTITLE
Optical Approaches for Drug Screening Based Light-Harvesting Conjugated Polyelectrolyte

5a. CONTRACT NUMBER
FA5209-08-P-0365

5b. GRANT NUMBER

5c. PROGRAM ELEMENT NUMBER

6. AUTHOR(S)
Bazan, Guillermo

5d. PROJECT NUMBER

5e. TASK NUMBER

5f. WORK UNIT NUMBER

7. PERFORMING ORGANIZATION NAME(S) AND ADDRESS(ES)
University of California, Santa Barbara
3227 Cheadle Hall
Santa Barbara, CA 93106-2050

8. PERFORMING ORGANIZATION REPORT NUMBER

9. SPONSORING/MONITORING AGENCY NAME(S) AND ADDRESS(ES)
United States Air Force, U.S. Army International Technology Center Pacific
374th Contracting Squadron
Unit 5228, Bldg 620
APO AP 96328-5228 United States

10. SPONSOR/MONITOR'S ACRONYM(S)
ITC-PAC

11. SPONSOR/MONITOR'S REPORT NUMBER(S)

12. DISTRIBUTION/AVAILABILITY STATEMENT
Approved for Public Release. Distribution Unlimited

20100617295

13. SUPPLEMENTARY NOTES

14. ABSTRACT
Multifunctional materials that can simultaneously provide therapeutic action and image the ensuing results provide new strategies for treating various diseases. In response, we have shown that a cationic conjugated polyelectrolyte with a molecular design containing a polythiophene–porphyrin dyad (PTP) has efficient anticancer and antifungal activities. Due to the light-harvesting ability of the electronically delocalized backbone and efficient energy transfer amongst the optical partners, the PTP shows a higher 1O2 generation efficiency and therefore improved therapeutic activity than a small molecule analog. Additionally, the fluorescent properties of PTP serve for another purpose, namely distinguishing amongst living and dead cells. PTP is therefore a promising multifunctional photosensitive agent for treating cancers and fungal infections, while concurrently providing optical monitoring capabilities.

15. SUBJECT TERMS
Conjugated polyelectrolytes (CPEs)

16. SECURITY CLASSIFICATION OF:			17. LIMITATION OF ABSTRACT	18. NUMBER OF PAGES	19a. NAME OF RESPONSIBLE PERSON
a. REPORT	b. ABSTRACT	c. THIS PAGE			Bazan, Guillermo
U	U	U	UU	31	19b. TELEPHONE NUMBER *(Include area code)* 805-893-5538

Final Technical Report

Optical Approaches for Drug Screening Based Light- Harvesting Conjugated Polyelectrolyte

PI: Dr. Guillermo Bazan

Introduction

Conjugated polyelectrolytes (CPEs) have been established as versatile macromolecules that can readily increase the sensitivity of fluorescent biosensors without the need for additional sophisticated instrumentation. Much of this work has been pioneered by the two research groups in this proposal.[1-7] Very briefly, the delocalized electronic structure of the CPE backbone can coordinates the action of a large number of absorbing units. Transfer of the excitation energy along the backbone and between chains results in the amplification of emission. The key transduction problem is to coordinate the energy transfer to a signaling dye upon a specific biomolecular recognition event. This challenge is usually overcome by coordinating electrostatic interactions. These considerations have led us to success in the amplification of PNA/ssDNA, ssDNA/ssDNA, protein/RNA, enzyme/substrate, and PNA/dsDNA recognition events.

The goals of the proposal were to extend our knowledge in photophysics, molecular design and self-assembly toward developing novel drug assay system based on CPEs. As a test example we will focus our work toward the problem of AIDS. New drugs against AIDS have been a challenge since the discovery of human immunodeficiency virus (HIV), which has infected more than 40 million people and led to nearly 3 million deaths worlds wide[8]. The sequence-specific interaction between the regulatory protein Rev and a portion of the env gene within the RNA gene (Rev responsive element, RRE) is critical for promoting HIV-1 replication; thus, disrupting and altering this essential interaction has been explored as a potentially novel approach for the development of new anti-HIV drugs [9,10].

References

1. B. Liu, G. C. Bazan, *Chem. Mater.* **2004**, *16*, 4467.
2. B. S. Gaylord, A. J. Heeger, G. C. Bazan, *Proc. Natl. Acid. Sci. USA* **2002**, *99*, 10954.
3. B. S. Gaylord, A. J. Heeger, G. C. Bazan, *J. Am. Chem. Soc.* **2003**, *125*, 896.
4. S. Wang, B. S. Gaylord, G. C. Bazan, *J. Am. Chem. Soc.* **2004**, *126*, 5446.
5. F. Feng, Y. Tang, F. He, M. Yu, X. Duan, S. Wang, Y. Li, D. Zhu, *Adv. Mater.* **2007**, *19*, 3490.
6. F. He, Y. Tang, S. Wang, Y. Li, D. Zhu, *J. Am. Chem. Soc.* **2005**, *127*, 12343.
7. F. He, Y. Tang, M. Yu, F. Feng, L. An, H. Sun, S. Wang, Y. Li, D. Zhu, G. C. Bazan, *J. Am. Chem. Soc.* **2006**, *128*, 6764.
8. C. Y. Zhang and L. W. Johnson, *Anal. Chem.* **2007**, *79*, 7775-7781.
9. S. R. Kirk, N. W. Luedtke and Y. Tor, *J. Am. Chem. Soc.* **2000**, *122*, 980-981.
10. E. S. DeJong, C. Chang, M. K. Gilson and J. P. Marino, *Biochemistry*, **2003**, *42*, 8035-8046

Background, Approach/methodology, Data/Results

Two nearly independent research efforts were concluded: (i) the use of conjugated polyelectrolytes as the optical platform for searching potential drug candidates and (ii) the demonstration of conjugated polyelectrolytes as useful agents for photodynamic therapy Major highlights and conclusions of the collaborative effort can be found on the two manuscripts, which are attached as Appendices A and B. Relevant background, introduction to each project and protocols used are also fully described.

Conclusion

Successful completion of the collaboration has demonstrated the enormous potential that conjugated polyelectrolytes can have in the design of high throughput protocols for searching potential dyes and as therapeutic and imaging agents for treating cancer via photodynamic therapy methods.

Highlights

It is worth pointing out that the scientific and technological outcome for this collaboration *far exceeds* the investment by the funding agencies. Part of the success stems from the mutually complementary expertise of the PIs and the previous demonstrated record of accomplishments.

From the perspective of the US Army, the outcome of the research pertains to ways to search for molecules that can be used as possible drug candidates and the development of materials that can be used to mitigate infections due to fungi.

The major challenge for the collaboration is to find funding lines that can support future growth of the projects. Most significantly, it would be appropriate for funds to be partitioned between the two institutions and to fund students in both places that can work together in a collaborative way.

Biosensors

DOI: 10.1002/anie.200900758

An Optical Approach for Drug Screening Based on Light-Harvesting Conjugated Polyelectrolytes**

Lingling An, Libing Liu, Shu Wang, and Guillermo C. Bazan**

Conjugated polyelectrolytes (CPEs) are water-soluble polymers that contain a π-delocalized backbone bearing pendant ionic functionalities. The polarizable electronic structure allows facile intra- or interchain migration of optical excitations; thus, it is possible to coordinate the action of a large number of absorbing units and obtain amplification of fluorescence signals relative to those of small-molecule dyes.[1,2] Furthermore, the charged groups allow electrostatic complexation and, thereby, can trigger of fluorescence resonance energy transfer (FRET) upon molecular-recognition events that change the net charge of the macromolecule bearing the reporter (acceptor) dye.[3,4] These features have allowed CPEs to function as the optical platform in highly sensitive chemical and biological sensors.[5–22]

In comparison to previous applications tailored for the detection of specific targets, we report herein on a different function: the use of CPEs for the real-time screening of potential drugs. Our strategy builds on specific RNA–protein interactions that mediate the replication cycles of pathogenic viruses, such as the human immunodeficiency virus type 1 (HIV-1) and picornaviruses.[23–25] Small organic molecules that target the viral RNA sites and thereby prevent RNA–protein complexation are sought as initial candidates for drug discovery.[26–31] Furthermore, CPEs can also be used as a key component for monitoring proteases that disturb recognition interactions by virtue of peptide-cleavage reactions.[10,21] These methods depart from traditional screening methods, such as gel shift mobility, NMR spectroscopy, or fluorescence assays,[26–29,32–34] which are time consuming and material intensive and which often require the labeling of multiple components.

To demonstrate the concept, the regulatory peptide (Rev) binding to the Rev responsive element (RRE) sequence in the RNA of HIV-1 was chosen as the RNA/peptide binding pair (see molecular structures in Scheme 1).[32] The stem–loop IIB of RRE RNA, which contains a purine-rich internal bulge, and a fluorescein (Fl) labeled Rev peptide with 17 amino acids (Rev-Fl) were used as the model for in vitro studies.[28,32] Poly{[(9,9-bis(6′-*N*,*N*,*N*-trimethylammonium)hexyl)-fluorenylene-phenylene] dibromide} (PFP) was used as the cationic CPE in the energy-transfer experiments. The absorption spectrum of the fluorescein (acceptor) overlaps with the emission of PFP (donor) and thus satisfies the conditions for efficient FRET. Furthermore, irradiation at 380 nm selec-

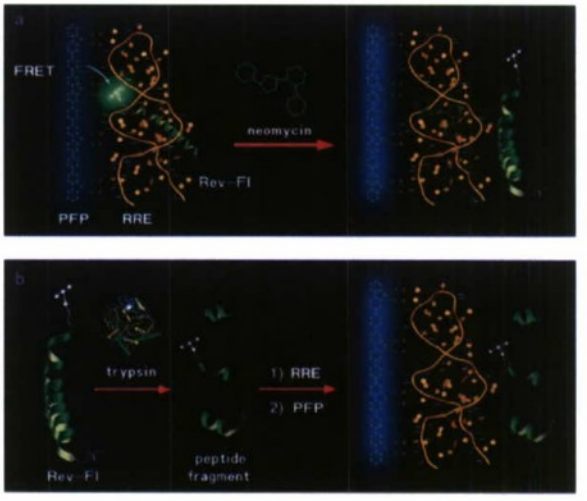

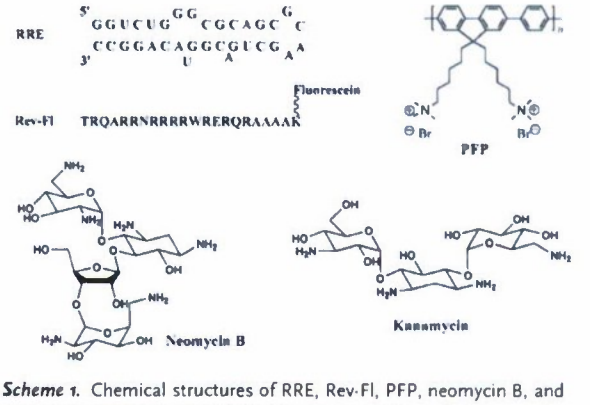

Scheme 1. Chemical structures of RRE, Rev-Fl, PFP, neomycin B, and kanamycin, together with schematic representations of a) the mechanism for detection of neomycin action and b) how digestion of Rev-Fl by trypsin leads to a reduction in FRET efficiency.

[*] L. An, Dr. L. Liu, Prof. S. Wang
Beijing National Laboratory for Molecular Sciences
Key Laboratory of Organic Solids, Institute of Chemistry
Chinese Academy of Sciences, Beijing, 100190 (P.R. China)
Fax: (+86) 10-6263-6680
E-mail: wangshu@iccas.ac.cn
Prof. G. C. Bazan
Departments of Chemistry and Materials
Center for Polymers and Organic Solids
University of California, Santa Barbara, CA 93106-9510 (USA)
E-mail: bazan@chem.ucsb.edu

[**] We are grateful to the "100 Talents" program of the Chinese Academy of Sciences, the National Natural Science Foundation of China (20725308 and 20721061), the National Basic Research Program of China (2006CB806200), the Major Research Plan of China (2006CB932102), the Institute for Collaborative Biotechnologies and the ITC-PAC (Contract No. FA5209-08-P-0365) University of California, Santa Barbara (UCSB), and the National Science Foundation (DMR 0606414).

InterScience
© 2009 Wiley-VCH Verlag GmbH & Co. KGaA, Weinheim

tively excites PFP. These features allow for simple evaluation of the FRET efficiencies between PFP and fluorescein.[6,8]

Scheme 1 diagrammatically shows the design and anticipated function of the PFP/Rev-Fl/RRE system. The arginine-rich Rev peptide is positively charged at neutral pH values. Upon addition of negatively charged RRE to a solution of Rev-Fl, the Rev-Fl/RRE complex forms and the *net* charge in this complex is negative. Addition of the cationic PFP results in formation of PFP/Rev-Fl/RRE electrostatic complexes, in which PFP resides in close proximity to fluorescein; the distance requirement for FRET is thus met. Neomycin B is a small-molecule antibiotic commonly used as a competitive inhibitor towards the RRE/Rev complex.[28,33] It is positively charged at neutral pH values and can bind to the major groove of duplex RNA through electrostatic interactions mediated by the ammonium groups. When neomycin is titrated into a PFP/RRE/Rev-Fl solution, the three-way binding equilibrium shifts toward the release of free Rev-Fl. This process results in the progressive removal of Rev-Fl from the vicinity of PFP and a concomitant reduction in FRET efficiency (Scheme 1a). Thus, PFP provides an optical and structural basis for modeling drug screening in a real-time fashion. Scheme 1b shows the anticipated function of trypsin, a serine protease that can cleave the Rev-Fl peptide on the C-terminal side of any lysine and arginine amino acid residues.[35] Breakdown of Rev-Fl generates short peptide fragments that do not associate with RRE. The reaction products also do not associate with PFP. Thus, digestion of Rev-Fl should also lead to an increase in the distance between the optical partners and a reduction in FRET efficiency.

Figure 1 compares the emission observed upon addition of PFP to a solution of Rev-Fl with RRE RNA. Also shown are the results when RRE RNA was replaced with a randomly chosen dsDNA to test the possibility of nonspecific binding. In these experiments, the Rev-Fl probe was premixed with the RRE RNA or dsDNA in buffer at 4°C; the concentrations of the reagents are given in the figure legend.[36] After addition of PFP, a comparison of the fluorescence intensities from the fluorescein upon excitation of PFP at 380 nm shows a larger FRET ratio with Rev-Fl/RRE than with the nonspecific Rev-Fl/dsDNA pair. Also shown are the results with PFP/Rev-Fl and PFP/RRE. These control experiments show that fluorescein is more efficiently sensitized by FRET from PFP when it is present in the Rev-Fl/RRE complex, that is, under conditions where the acceptor is found in a macromolecule with net negative charge.

Two aminoglycoside antibiotics, neomycin B and kanamycin, which are competitive inhibitors towards RRE–Rev complexation, albeit with different binding efficiencies, were selected to study how the PFP/Rev-Fl/RRE system can be used to screen small molecules that inhibit Rev–RRE interactions. In these experiments, solutions containing Rev-Fl and RRE were incubated at 4°C for 15 minutes in buffer; this was followed by the addition of PFP and then different concentrations of neomycin B. After incubation of the mixture at 4°C for 2 minutes, the fluorescence spectra were measured upon excitation of PFP at 380 nm. As shown in Figure 2a, addition of neomycin B in the concentration range from 0 up to 2.2 mM leads to a progressive increase in the emission intensity of PFP at 425 nm (I_{425nm}) and a decrease in fluorescein emission at 526 nm (I_{526nm}). From Figure 2b, we can see that, when [neomycin B] = 2.2 mM, the ratio of the intensity at 425 nm versus that at 526 nm increases approximately seven-fold. These experiments show that the addition of neomycin B into the PFP/RRE/Rev-Fl system causes

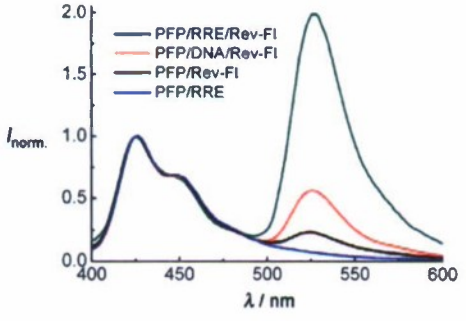

Figure 1. Emission spectra from solutions containing PFP with RRE/Rev-Fl (green line), double-stranded (ds) DNA/Rev-Fl (red line), RRE (blue line), and Rev-Fl (black line). Conditions: [PFP] = 4.0×10^{-7} M in repeat units (RUs), [RRE] = [Rev-Fl] = 1.0×10^{-8} M, [dsDNA] = 6.8×10^{-9} M (in strands). Measurements were performed at 4°C in a buffer solution (pH 7.4) containing 20 mM 2-[4-(2-hydroxyethyl)-1-piperazinyl]ethanesulfonic acid (HEPES), 5 mM KCl, 1 mM $CaCl_2$, 1 mM $MgCl_2$, and 140 mM NaCl. The excitation wavelength was 380 nm. Spectra are normalized with respect to PFP emission for ease of comparison.

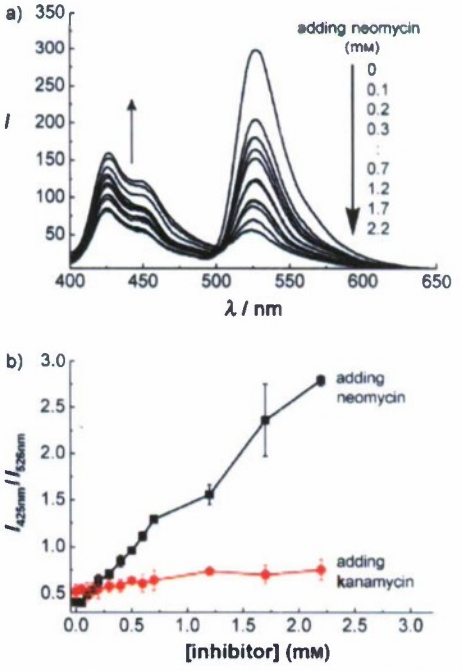

Figure 2. a) Emission spectra of PFP/RRE/Rev-Fl as a function of neomycin B concentration. [Neomycin] = 0.0–2.2 mM. b) I_{425nm}/I_{526nm} ratio of PFP/RRE/Rev-Fl as a function of the antibiotic concentration. [Neomycin] = [Kanamycin] = 0.0–2.2 mM, [PFP] = 4.0×10^{-7} M in RUs, [RRE] = [Rev-Fl] = 1.0×10^{-8} M. Measurements were performed at 4°C in a buffer solution (pH 7.4) containing 20 mM HEPES, 5 mM KCl, 1 mM $CaCl_2$, 1 mM $MgCl_2$, and 140 mM NaCl. The excitation wavelength was 380 nm. The error bars represent the standard deviation of triplicate measurements.

© 2009 Wiley-VCH Verlag GmbH & Co. KGaA, Weinheim

displacement of Rev-Fl from the complex and disturbs the energy-transfer process. It is also significant that kanamycin only leads to a negligible change of the I_{425nm}/I_{526nm} ratio under similar experimental conditions to those used with neomycin B (Figure 2b). The much larger change in the I_{425nm}/I_{526nm} ratio with neomycin B, relative to that with kanamycin, is related to its more efficient inhibition of Rev–RRE complexation (dissociation constant $K_d = 2.2 \times 10^{-7}$ M for neomycin B; $K_d = 2.5 \times 10^{-5}$ M for kanamycin).[33b] Thus, the PFP/RRE/Rev-Fl system provides a sensitive, rapid, and convenient protocol to screen promising small-molecule leads for anti-HIV drugs.

We now examine how digestion of the Rev fragment by trypsin influences the collective optical response. In these experiments, a solution containing Rev-Fl and trypsin is first incubated at 37 °C for a specific period of time. RRE is then added, and the resulting solution is allowed to incubate at 4 °C for 4 minutes. The final step involves addition of PFP and measurement of the fluorescence spectra upon excitation at 380 nm. As shown in Figure 3a, the emission intensity of PFP at 425 nm increases and that of fluorescein at 526 nm decreases as the trypsin-incubation time increases from 0 to 21 minutes. Hydrolysis of Rev-Fl catalyzed by trypsin thus leads to easily distinguishable optical signatures from the PFP/Rev-Fl/RRE system and is consistent with the overall mechanism proposed in Scheme 1b. Furthermore, the I_{425nm}/I_{526nm} ratio can be related to the population of cleaved Rev fragments. This feature can be used to evaluate the trypsin activity, as illustrated in Figure 3b, which shows the I_{425nm}/I_{526nm} values as a function of [trypsin] and digestion time. That larger I_{425nm}/I_{526nm} ratios are observed with higher trypsin concentrations provides evidence of the faster cleavage reaction rates and demonstrates the viability of this method for evaluating enzyme activity. Control experiments were also done with the nonspecific proteins bovine serum albumin (BSA) and butyrylcholinesterase (BchE). As shown in Figure 3c, there is virtually no change in the I_{425nm}/I_{526nm} value with BSA and BchE, which is consistent with the specific cleavage of Rev-Fl by trypsin. It is also interesting to note that nonspecific PFP–protein interactions that can lead to perturbations in fluorescence are not significant within this set of reactants.[37] The collected evidence is consistent with specific cleavage of Rev-Fl by trypsin controlling the change in the I_{425nm}/I_{526nm} value; these results highlight the potential of the PFP/Rev-Fl/RRE platform for screening potential enzyme agents that target recognition peptides.

We have thus demonstrated how to integrate CPE materials into assays for screening agents that disturb critical recognition events in viral replication cycles. Hits in these assays constitute a preliminary, but vital, step forward in the search for new small molecules or proteins that have therapeutic potential. The method in Scheme 1 incorporates the inhibition of specific RNA–protein (RRE–Rev) interactions, in combination with the light-harvesting properties of CPEs. We recognize that the nature of the CPE/RNA/protein complexes most likely involves higher order aggregates, rather than well-defined ternary systems as depicted in Scheme 1.[38] Regardless of these uncertainties, the CPE-based detection protocol offers several significant practical

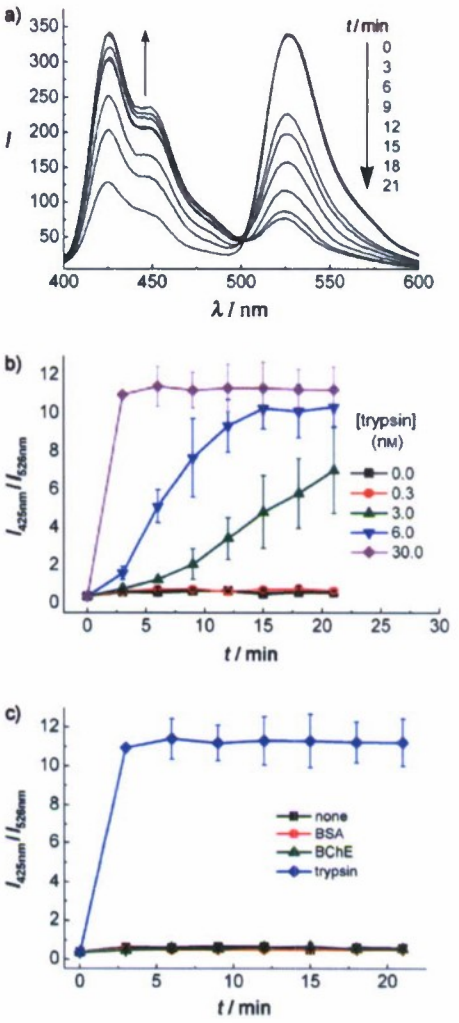

Figure 3. a) Emission spectra of PFP/RRE/Rev-Fl as a function of trypsin digestion time. The final concentration of trypsin is 3.0 nM. b) Plot of I_{425nm}/I_{526nm} versus digestion time with various trypsin concentrations. The final concentration of trypsin is 0.0–30 nM. c) Plot of I_{425nm}/I_{526nm} versus digestion time in the presence of trypsin and nonspecific proteins. Final concentrations: [protein] = 30 nM, [PFP] = 4.0×10^{-7} M in RUs, [RRE] = [Rev-Fl] = 1.0×10^{-8} M. Measurements were performed at 4 °C in buffer solution (pH 7.4) containing 20 mM HEPES, 5 mM KCl, 1 mM $CaCl_2$, 1 mM $MgCl_2$, and 140 mM NaCl. The excitation wavelength was 380 nm. Error bars represent the standard deviation of triplicate measurements.

features. First, it offers a convenient "mix-and-detect" approach for the rapid screening of small molecules. Second, the CPE offers significant amplification of the detection signal, which imparts assays with high sensitivity. Third, in contrast to reported FRET-based methods, our strategy does not require labeling of the RNA probes, which should reduce costs. Furthermore, such fluorescence screening systems could be expanded to high-throughput protocols. Additionally, the successful evaluation of the action of trypsin promises to expand the function of CPE materials into the monitoring of protease activity. The composite set of properties is general and should be straightforward to adapt not only

 © 2009 Wiley-VCH Verlag GmbH & Co. KGaA, Weinheim

to screening anti-HIV chemical and biological molecules with abilities to disrupt and alter specific RRE–Rev interactions but also to the targeting of other important pathogens in viral and bacterial diseases.[39]

Experimental Section

Materials and measurements: The RRE RNA and oligonucleotide DNA were custom made by TaKaRa Biotechnology Co. Ltd. (Dalian), and their concentrations were determined by measuring the absorbance at 260 nm in 200 μL quartz cuvettes. The RNA was renatured by incubation in a buffer solution (pH 7.4) containing 20 mM HEPES, 5 mM KCl, 1 mM $CaCl_2$, 1 mM $MgCl_2$, and 140 mM NaCl for 2 min at 90 °C, followed by slow cooling to room temperature. The polypeptide modified by fluorescein on the N terminus (Rev-Fl) was made by GL Biochem Ltd. (Shanghai), and its concentration was determined by measuring the absorbance at 280 nm in 200 μL quartz cuvettes. Neomycin B and kanamycin were purchased from Amresco and used without further purification. PFP was prepared according to literature procedure.[6] UV/Vis absorption spectra were taken on a JASCO V-550 spectrophotometer. Fluorescence measurements were recorded on a Hitachi F-4500 spectrophotometer equipped with a xenon-lamp excitation source. All fluorescence spectra were measured at an excitation wavelength of 380 nm. Water was purified by using a Millipore filtration system.

Trypsin cleavage assays: Rev-Fl (2.5 μM) was added into 5 buffer solutions (20 mM HEPES, 5 mM KCl, 1 mM $CaCl_2$, 1 mM $MgCl_2$, and 140 mM NaCl, pH 7.4) with a total volume of 30 μL each, and then trypsin was added to each in various amounts (0, 0.3, 3.0, 6.0, or 30.0 nM). The samples were incubated at 37 °C, and after a specific incubation period, aliquots (4.0 μL) of the solutions were drawn out and diluted to 1000 μL with buffer containing RRE (1.0×10^{-8} M). After incubation for 4 min at 4 °C, PFP ([PFP] = 4.0×10^{-7} M in RUs) was added, and the fluorescence spectra were recorded at 4 °C. Plots of the fluorescence-intensity ratio (I_{425nm}/I_{526nm}) versus the incubation time were then obtained.

Inhibitor screening: A 3 mL plastic cuvette containing RRE (1.0×10^{-8} M) and Rev-Fl (1.0×10^{-8} M) in buffer solution (20 mM HEPES, 5 mM KCl, 1 mM $CaCl_2$, 1 mM $MgCl_2$, and 140 mM NaCl, pH 7.4) was incubated for 15 min at 4 °C. After incubation, PFP was added to the cuvette ([PFP] = 4.0×10^{-7} M in RUs). Neomycin B was then added successively (0.0–2.2 mM) at 4 °C, and the fluorescence spectra were measured. Plots of the fluorescence-intensity ratio (I_{425nm}/I_{526nm}) versus the incubation time were then obtained. The assay procedure for kanamycin was same as that for neomycin B except that kanamycin was used in place of neomycin B.

Received: February 8, 2009
Published online: May 13, 2009

Keywords: biosensors · conjugated polyelectrolytes · drug screening · FRET

[1] S. W. Thomas III, G. D. Joly, T. M. Swager, *Chem. Rev.* **2007**, *107*, 1339.
[2] T. Q. Nguyen, J. J. Wu, V. Doan, B. J. Schwartz, S. H. Tolbert, *Science* **2000**, *288*, 652.
[3] B. Liu, G. C. Bazan, *Chem. Mater.* **2004**, *16*, 4467.
[4] F. Feng, F. He, L. An, S. Wang, Y. Li, D. Zhu, *Adv. Mater.* **2008**, *20*, 2959.
[5] J. H. Wosnick, C. M. Mello, T. M. Swager, *J. Am. Chem. Soc.* **2005**, *127*, 3400.
[6] B. S. Gaylord, A. J. Heeger, G. C. Bazan, *Proc. Natl. Acad. Sci. USA* **2002**, *99*, 10954.
[7] D. Wang, X. Gong, P. S. Heeger, F. Rininsland, G. C. Bazan, A. J. Heeger, *Proc. Natl. Acad. Sci. USA* **2002**, *99*, 49.
[8] S. Wang, B. S. Gaylord, G. C. Bazan, *J. Am. Chem. Soc.* **2004**, *126*, 5446.
[9] S. Kumaraswamy, T. S. Bergstedt, X. Shi, F. Rininsland, S. A. Kushon, W. Xia, K. D. Ley, K. E. Achyuthan, D. McBranch, D. G. Whitten, *Proc. Natl. Acad. Sci. USA* **2004**, *101*, 7511.
[10] a) I. B. Kim, B. Erdogan, J. N. Wilson, U. H. F. Bunz, *Chem. Eur. J.* **2004**, *10*, 6247; b) R. L. Phillips, O. R. Miranda, C. C. You, V. M. Rotello, U. H. F. Bunz, *Angew. Chem.* **2008**, *120*, 2628; *Angew. Chem. Int. Ed.* **2008**, *47*, 2590; c) C. C. You, O. R. Miranda, B. Gider, P. S. Ghosh, I. B. Kim, B. Erdogan, S. A. Krovi, U. H. F. Bunz, V. M. Rotello, *Nat. Nanotechnol.* **2007**, *2*, 318.
[11] C. Y. J. Yang, M. R. Pinto, K. S. Schanze, W. H. Tan, *Angew. Chem.* **2005**, *117*, 2628; *Angew. Chem. Int. Ed.* **2005**, *44*, 2572.
[12] M. R. Pinto, K. S. Schanze, *Proc. Natl. Acad. Sci. USA* **2004**, *101*, 7505.
[13] H. Xu, H. Wu, F. Huang, S. Song, W. Li, Y. Cao, C. Fan, *Nucleic Acids Res.* **2005**, *33*, e83.
[14] K. Lee, J.-M. Rouillard, T. Pham, E. Gulari, J. Kim, *Angew. Chem.* **2007**, *119*, 4751; *Angew. Chem. Int. Ed.* **2007**, *46*, 4667.
[15] H. A. Ho, A. Najari, M. Leclerc, *Acc. Chem. Res.* **2008**, *41*, 168.
[16] H. A. Ho, M. Boissinot, M. G. Bergeron, G. Corbeil, K. Doré, D. Boudreau, M. Leclerc, *Angew. Chem.* **2002**, *114*, 1618; *Angew. Chem. Int. Ed.* **2002**, *41*, 1548.
[17] K. P. R. Nilsson, O. Inganäs, *Nat. Mater.* **2003**, *2*, 419.
[18] C. J. Sigurdson, K. P. R. Nilsson, S. Hornemann, G. Manco, M. Polymenidou, P. Schwarz, M. Leclerc, P. Hammarström, K. Wüthrich, A. Aguzzi, *Nat. Methods* **2007**, *4*, 1023.
[19] C. Li, M. Numata, M. Takeuchi, S. Shinkai, *Angew. Chem.* **2005**, *117*, 6529; *Angew. Chem. Int. Ed.* **2005**, *44*, 6371.
[20] F. Feng, H. Wang, L. Han, S. Wang, *J. Am. Chem. Soc.* **2008**, *130*, 11338.
[21] F. Feng, Y. Tang, S. Wang, Y. Li, D. Zhu, *Angew. Chem.* **2007**, *119*, 8028; *Angew. Chem. Int. Ed.* **2007**, *46*, 7882.
[22] Y. Tang, F. Feng, F. He, S. Wang, Y. Li, D. Zhu, *J. Am. Chem. Soc.* **2006**, *128*, 14972.
[23] G. Varani, *Acc. Chem. Res.* **1997**, *30*, 189.
[24] B. A. Sullenger, E. Gilboa, *Nature* **2002**, *418*, 252.
[25] E. V. Pilipenko, T. V. Pestova, V. G. Kolupaeva, E. V. Khitrina, A. N. Poperechnaya, V. I. Agol, *Genes Dev.* **2000**, *14*, 2028.
[26] Y. Jin, J. A. Cowan, *J. Am. Chem. Soc.* **2006**, *128*, 410.
[27] S. R. Kirk, N. W. Luedtke, Y. Tor, *J. Am. Chem. Soc.* **2000**, *122*, 980.
[28] a) E. S. DeJong, C. Chang, M. K. Gilson, J. P. Marino, *Biochemistry* **2003**, *42*, 8035; b) M. L. Zapp, S. Stern, M. R. Green, *Cell* **1993**, *74*, 969.
[29] K. Moehle, Z. Athanassiou, K. Patora, A. Davidson, G. Varani, J. A. Robinson, *Angew. Chem.* **2007**, *119*, 9260; *Angew. Chem. Int. Ed.* **2007**, *46*, 9101.
[30] Y. Lee, S. Hyun, H. J. Kim, J. Yu, *Angew. Chem.* **2008**, *120*, 140; *Angew. Chem. Int. Ed.* **2008**, *47*, 134.
[31] T. Hermann, *Angew. Chem.* **2000**, *112*, 1962; *Angew. Chem. Int. Ed.* **2000**, *39*, 1890.
[32] C.-Y. Zhang, L. W. Johnson, *J. Am. Chem. Soc.* **2006**, *128*, 5324.
[33] a) K. A. Lacourciere, J. T. Stivers, J. P. Marino, *Biochemistry* **2000**, *39*, 5630; b) N. W. Luedtke, Q. Liu, Y. Tor, *Biochemistry* **2003**, *42*, 11391.
[34] N. W. Luedtke, Y. Tor, *Biopolymers* **2003**, *70*, 103.
[35] M. F. Kircher, R. Weissleder, L. A. Josephson, *Bioconjugate Chem.* **2004**, *15*, 242.
[36] R. Tan, L. Chen, J. A. Buettner, D. Hudson, A. D. Frankel, *Cell* **1993**, *73*, 1031.
[37] S. J. Dwight, B. S. Gaylord, J. W. Hong, G. C. Bazan, *J. Am. Chem. Soc.* **2004**, *126*, 16850.
[38] C. Y. Chi, A. Chworos, J. P. Zhang, A. Mikhailovsky, G. C. Bazan, *Adv. Funct. Mater.* **2008**, *18*, 3606.
[39] Y. Tor, *Angew. Chem.* **1999**, *111*, 1681; *Angew. Chem. Int. Ed.* **1999**, *38*, 1579.

 © 2009 Wiley-VCH Verlag GmbH & Co. KGaA, Weinheim

Conjugated polyelectrolytes with imaging capabilities for light-activated anticancer and antifungal activity

Chengfen Xing[1], Libing Liu[1]*, Hongwei Tang[1], Xuli Feng[1], Qiong Yang[1], Shu Wang[1]*, Guillermo C. Bazan[2]*

[1]Beijing National Laboratory for Molecular Sciences, Key Laboratory of Organic Solids, Institute of Chemistry, Chinese Academy of Sciences, Beijing, 100190, P. R. China.

E-mail: wangshu@iccas.ac.cn; liulibing@iccas.ac.cn

[2]Departments of Chemistry & Biochemistry and Materials, Center for Polymers and Organic Solids, University of California, Santa Barbara, CA 93106-9510, USA

E-mail: bazan@chem.ucsb.edu

Abstract

Multifunctional materials that can simultaneously provide therapeutic action and image the ensuing results provide new strategies for treating various diseases. Here, we show that a cationic conjugated polyelectrolyte with a molecular design containing a polythiophene–porphyrin dyad (PTP) has efficient anticancer and antifungal activities. Upon photoexcitation, energy is efficiently transferred from the polythiophene backbone to the porphyrin units, which readily produce singlet oxygen ($^1O_2$) for rapidly killing neighboring cancer cells and fungi. Due to the light-harvesting ability of the electronically delocalized backbone and efficient energy transfer amongst the optical partners, the PTP shows a higher $^1O_2$ generation efficiency and therefore improved therapeutic activity than a small molecule analog. Additionally, the fluorescent properties of PTP serve for another purpose, namely distinguishing amongst living and dead cells. PTP is therefore a promising multifunctional photosensitive agent for treating cancers and fungal infections, while concurrently providing optical monitoring capabilities. These findings illustrate new directions for the design of synthetic multipurpose water-soluble polymers.

Conjugated polymers are characterized by a delocalized π-electronic backbone structure and large optical absorption coefficients. Facile energy transfer along the backbone and between chains allows excitations to sample a larger number of environments in comparison to isolated small molecules.[1] Photoexcitations can be channeled to suitable adjacent acceptors by fluorescence resonance energy transfer (FRET) mechanisms, leading to sensitization of emitters to levels above those attained by direct excitation. Conjugated polyelectrolytes incorporate charged groups onto the conjugated polymer backbone. Such a structural modification improves solubility in aqueous media, an important requirement for interacting with biological systems and for the design of optically amplified fluorescent biosensors.[2]

Acceptor molecules can be chosen to have optoelectronic properties that increase FRET efficiencies.[3] Conjugated polyelectrolyte/acceptor systems have therefore gained much recent attention for applications in detection and cell imaging.[4-9] Energy transfer to porphyrin acceptors can be chosen to harness excitations for generating reactive oxygen species[10-13] and to open potential applications in photodynamic therapy (PDT).[14] Based on these unique properties, conjugated polyelectrolyte/acceptor materials can be expected to act as both therapeutic and imaging agents in therapy. The imaging function is particularly significant when it is capable of monitoring and guiding treatment. Integration of imaging modalities with therapeutic function within a single bio-compatible material is therefore anticipated to increase in importance as a new and challenging design element.[15,16]

The use of PDT for fungal infections is also an emerging relevant topic on account of the increasing resistance to multiple conventional antifungal agents, which results in the recurrence of the infection and prolonged treatments.[17] Fungi are more resistant to PDT, as

compared to gram-negative bacteria, since their more rigid cell walls increase the barrier for drug penetration. Higher doses of light and photosensitizer concentrations are therefore required.[18] Although new efficient antifungal photosensitizers have been developed, their toxicity limits their application in PDT.[19,20] New alternative antifungal strategies and the design of multifunctional optical materials are therefore of interest.

Here, we describe the synthesis and application of a cationic conjugated polythiophene–porphyrin dyad (PTP) that was specifically designed to concurrently act as a therapeutic and an imaging agent. Four significant characteristics were included in the molecular design shown in **Scheme 1**. First, the fractional content of porphyrin moieties linked to the polythiophene backbone is low (~ 1%), in order to minimize toxicity in the absence of photoexcitation. Second, the amphiphilic attributes of PTP were anticipated to promote adsorption to cells and fungi through a combination of electrostatic and hydrophobic binding forces. Furthermore, PTP self-assembles in aqueous media into nanoparticles with appropriate dimensions for improved uptake into cancer cells. Third, covalent attachment of porphyrin moieties to the light harvesting polythiophene backbone constrains the interchromophore distances for optimizing FRET. This design element is important for increasing the photoconversion efficiency of singlet oxygen ($^1O_2$) generation. A practical consequence is that the conjugated polymer reduces the light intensity required to attain a target $^1O_2$ concentration. Fourth, because the PTP backbone retains emission, it can also be used to monitor apoptosis and necrosis processes by fluorescence imaging, adding a new dimension to the function of the molecular construct. Such simultaneous imaging and PDT function extend the applications of water-soluble conjugated polymers beyond their

established biosensing capabilities.

Scheme 1 illustrates the mechanism of anticancer activity by PTP. The positively charged and amphiphilic structure of PTP promotes membrane adsorption and subsequent uptake into the interior of the cell. Under light irradiation, there is efficient energy transfer from the polythiophene backbone to the pendant porphyrin sites, followed by sensitization of oxygen to generate $^1O_2$. This generated $^1O_2$ is toxic to the cells.

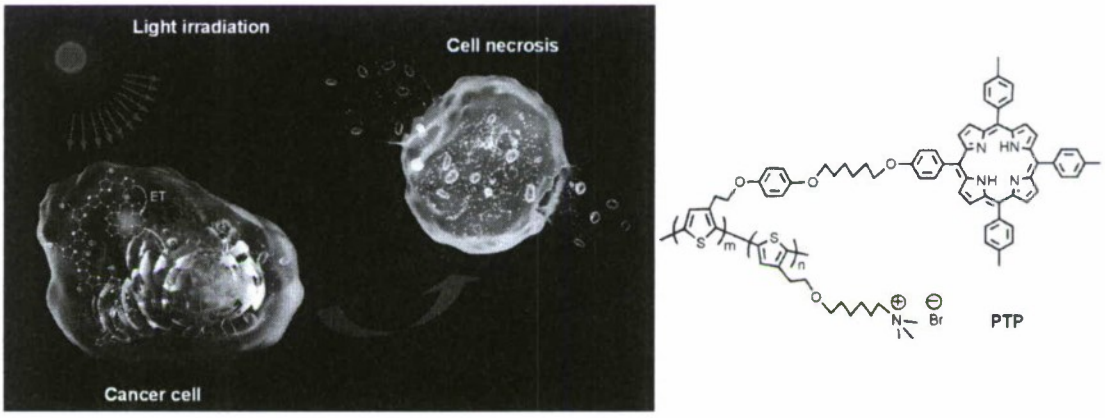

Scheme 1. Chemical structure of PTP and a schematic mechanism of PTP anticancer activity under irradiation. Components in the cell are not to scale.

Scheme 2 shows the synthesis of PTP, complete details can be found in the Supporting Materials. Reaction of pyrrole, 4-(6-bromohexyloxy)benzaldchyde (**1**)[21] and *p*-tolualdehyde (**2**) in the presence of BF_3-diethyl ether in $CHCl_3$, followed by treatment with 2,3-dichloro-5,6-dicyanobenzoquinone (DDQ) affords the porphyrin derivative **3**. Treatment of **3** with 30% trimethylamine-methanol solution provides the cationic porphyrin derivative TPN. Monomer **6** was prepared by reaction of 2-(3-thienyl)-ethanol tosylate (**4**) and hydroquinone, followed by reaction with **3**. Reaction of 2-(thiophen-3-yl)ethanol (**7**) with 1,6-dibromohexane in the presence of sodium hydride in dry DMF under nitrogen affords

3-(2-(6-bromohexyloxy)ethyl)thiophene (**8**) in 31% yield. Subsequent conversion to 6-(2-(thiophen-3-yl)ethoxy)hexyltrimethylammonium bromide (**9**) is accomplished in 89% yield by reaction with excess trimethylamine in methanol. The cationic polythiophene PT was obtained through oxidative polymerization of **9** in chloroform using $FeCl_3$, followed by purification by dialysis in water. Monomers **6** and **9** undergo oxidative copolymerization under nitrogen in the presence of $FeCl_3$ to give the target cationic porphyrin-containing polythiophene (PTP). The molar feed ratio of monomer of **6** to **9** is 1:10 and the actual porphyrin content in PTP was determined to be ~1% by examination of the absorption spectrum (**Figure S1**).

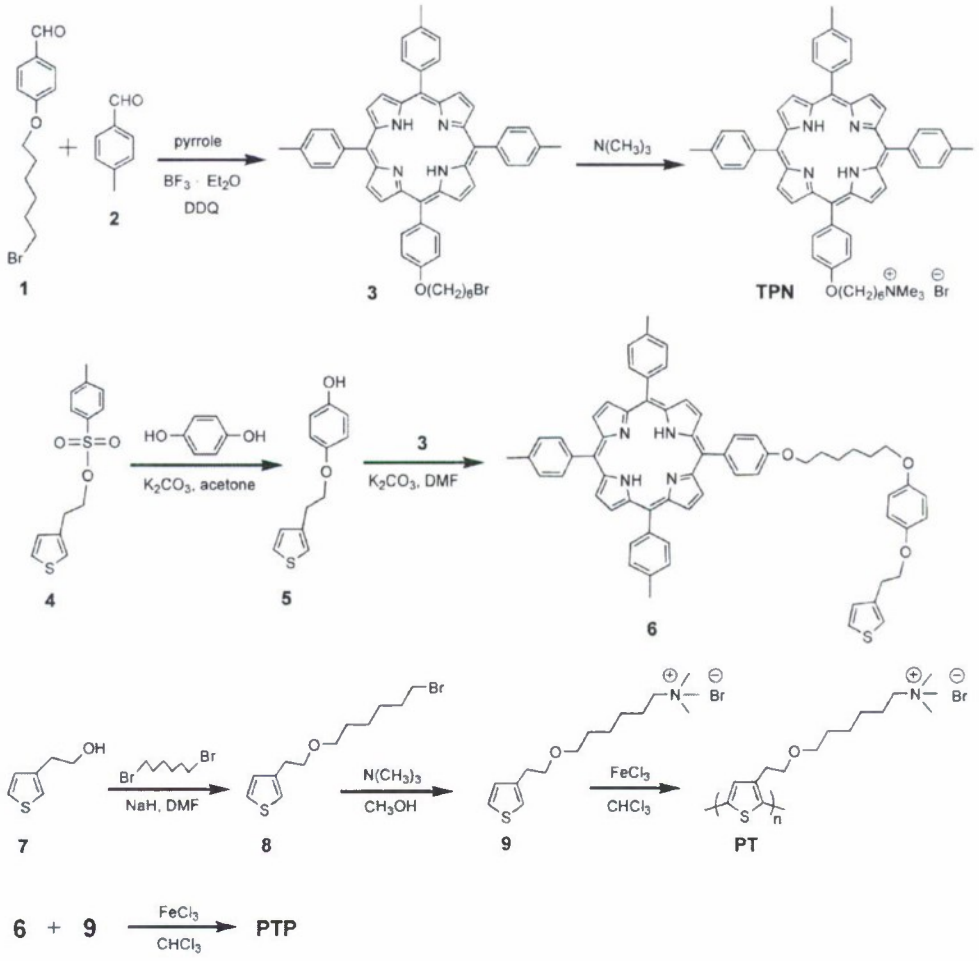

Scheme 2. Synthetic preparations of TPN, PT and PTP.

The photophysical properties of PTP, PT and TPN were investigated in aqueous solution, and the most relevant results are shown in **Figure 1a** and **1b**. For TPN, the absorption spectra exhibit a Soret band at 420 nm and Q bands between 520 nm and 670 nm; the emission spectrum shows a maximum peak at 655 nm with a fluorescence quantum yield (QY) of 1 %. For PT, the absorption maximum is at around 420 nm, corresponding to the π–π^* transition of the conjugated backbone; emission displays a maximum at 578 nm and occurs with a QY of 2 %. The absorption spectrum of PTP incorporates features common to the PT backbone and the porphyrin units. Excitation of PTP at 470 nm, where the porphyrin units do not absorb, leads to emission with peaks at 578 nm and 658 nm with a QY of 2 %. That a peak is observed at 658 nm demonstrates efficient energy transfer from polythiophene units to the porphyrin sites. It is also relevant to note that PTP aggregates in aqueous solution. Dynamic light scattering (DLS) measurement shows that the average particle size is approximately 350 nm (**Figure 1c**), which is appropriate for uptake into cells.[22,23]

Relative $^1O_2$ photogeneration efficiencies by the different photosensitizers were probed by measuring the conversion of disodium 9,10-anthracenedipropionic acid (ADPA)[24] to its endoperoxide via the corresponding decrease of the absorption band at 378 nm. PTP, TPN and PT were compared upon exposure to white light (400–800 nm), and the results are summarized in **Figure 1d**. In these experiments, the concentrations of PT and PTP were 10 μM in terms of polymer repeat units (RUs), and the concentration of TPN (0.15 μM) was similar to that of the pendant porphyrin units in the PTP solutions. The first order plots of the decrease of ADPA absorption at 378 nm as a function of irradiation time[13] show a

considerably faster disappearance upon photoexcitation of PTP. The observed rate constants of ADPA consumption in the presence of PTP, PT and TPN are 1.25 $\times 10^{-2}$, 2.7 $\times 10^{-3}$ and 7.3 $\times 10^{-5}$ s^{-1}, respectively. Thus, the bleaching rate of ADPA with PTP is 170 fold faster than that with TPN and ~ 5 fold faster than that with PT. These results show that the covalent attachment of porphyrin moieties onto PTP yields a synergistic improvement relative to the isolated PT or TPN components, and are consistent with energy transfer from the polythiophene backbone to the porphyrin sites, which significantly increases the $^1O_2$ generation efficiency (also see Figure S2).

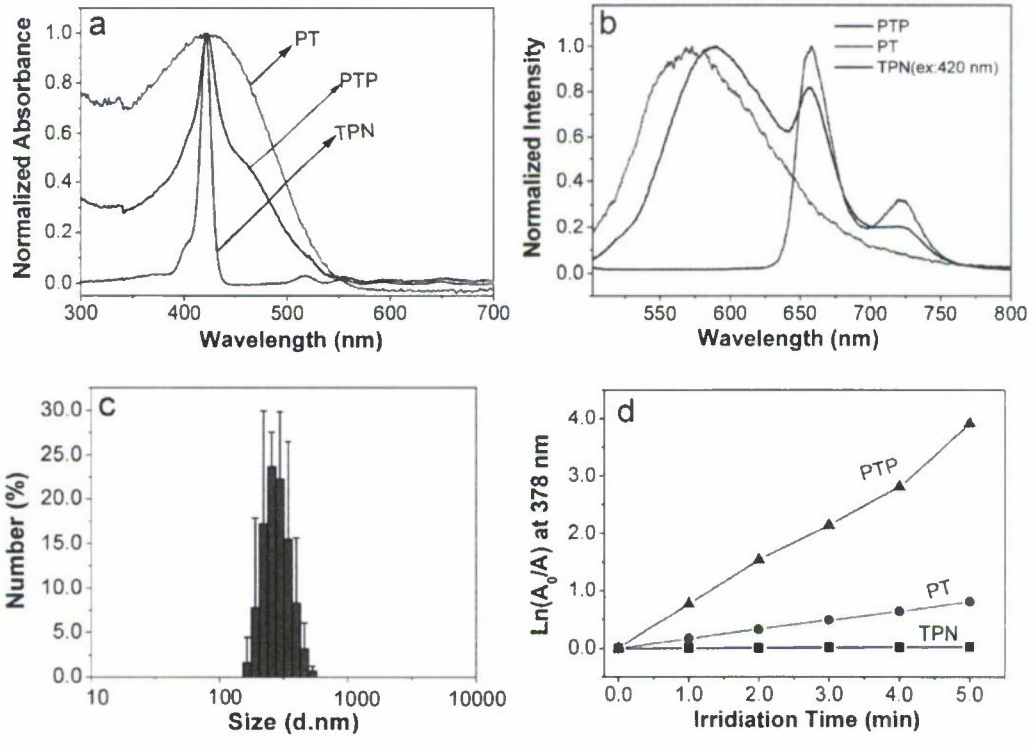

Figure 1. Photophysical properties of PTP, PT and TPN, structural characterization of PTP aggregation in water, and comparison of $^1O_2$ generation efficiencies. (a) Normalized UV-vis absorption spectra of PTP, PT and TPN in aqueous solution. (b) Normalized emission spectra of PTP, PT and TPN in aqueous solution. PT and TPN were excited at 420 nm and PTP at 470 nm. (c) Dynamic light scattering analysis of PTP aggregates in aqueous solution. (d) Decrease of ADPA absorption at 378 nm as a function of light irradiation time in the presence

of TPN, PT and PTP in D_2O solution. [PTP] = [PT] = 10 μM in RUs, [TPN] = 0.15 μM and [ADPA] =120 μM. A_0 is the absorbance of ADPA at 378 nm before irradiation, and A is that after irradiation with white light (400-800 nm). Values represent subtraction of the residual bleaching data of ADPA alone under the same irradiation condition.

The ability of PTP to generate $^1O_2$ was anticipated to induce oxidative stress and trigger apoptosis, necrosis or autophagy-associated cell death.[25] Two kinds of cancer cells, pulmonary adenocarcinoma cell (A549) and renal cell carcinoma (A498), were used as initial targets. The morphologies of A498 cancer cells in the presence of PTP after different periods of illumination were examined by phase contrast and fluorescence microscopy. For these experiments, plates containing A498 cells were irradiated at 470 nm for 0, 10 and 30 min, respectively, ethidium bromide (EB), which only stains apopotic or dead cells, was then added. Resulting samples were examined by fluorescence microscopy by excitation at 470 nm to selectively excite the polythiophene backbone. As shown by the phase contrast bright-field images in **Figure 2a**, irradiation leads to cell morphology changes that include chromatin compaction, cytoplasm condensation, and especially a large amount of blebbing. After 30 min irradiation, whole-cell shrinkage takes place. Persistent volume reduction is a major hallmark of cell death.[26,27] These results are corroborated by the overlapping fluorescence images of A498 cells in the presence of PTP and EB, where the amount of EB-stained dead cells has increased in tandem with prolonged irradiation time.

As shown in **Figure 2b**, imaging the location of PTP emission can be used to distinguish between living and dead cells. In living cells, the PTP emission is largely located in the cytoplasm. For dead cells, one observes translocation such that the PTP fluorescence now

takes place within the nucleus. Correlation with the fluorescence from EB-stained cells confirms assignment of dead cells.

Cytotoxicities of PTP, PT and TPN toward the A498 and A549 cancer cells were determined by using a standard assay in which the conversion of MTT (3-(4,5-dimethylthiazol-2-yl)-2,5-diphenyl-2H-tetrazolium hydrobromide) into formazan is related to mitochondrial activity and thus cell viability.[28] The PDT treatment was performed by illumination at 470 nm for 30 min. As shown in **Figure 2c**, under illumination, PTP displays more prominent cytotoxicity than PT at similar repeat unit concentrations, and TPN (normalized to the molar quantity of pendant porphyrin units). Also noteworthy is that PTP exhibits very low dark cytotoxicity, which is similar to PT and TPN (**Figure S3**). Moreover, a lower light dose at a fluence rate of 1.4 $mW \cdot cm^{-2}$ for 30 min of irradiation (2.5 $J \cdot cm^{-2}$) is used in our PDT experiment, in comparison to other approved photosensitizers,[16,29,30] thus PTP shows a realistic potential for application in photodynamic cancer therapy. We also examined the decrease of A498 cell viability with increasing light exposure time by the MTT assay (**Figure 2c**) at [PTP] = 10 μM RUs. The results show that cell viability decreases with increasing illumination time and that significant cell death is induced after 30 min.

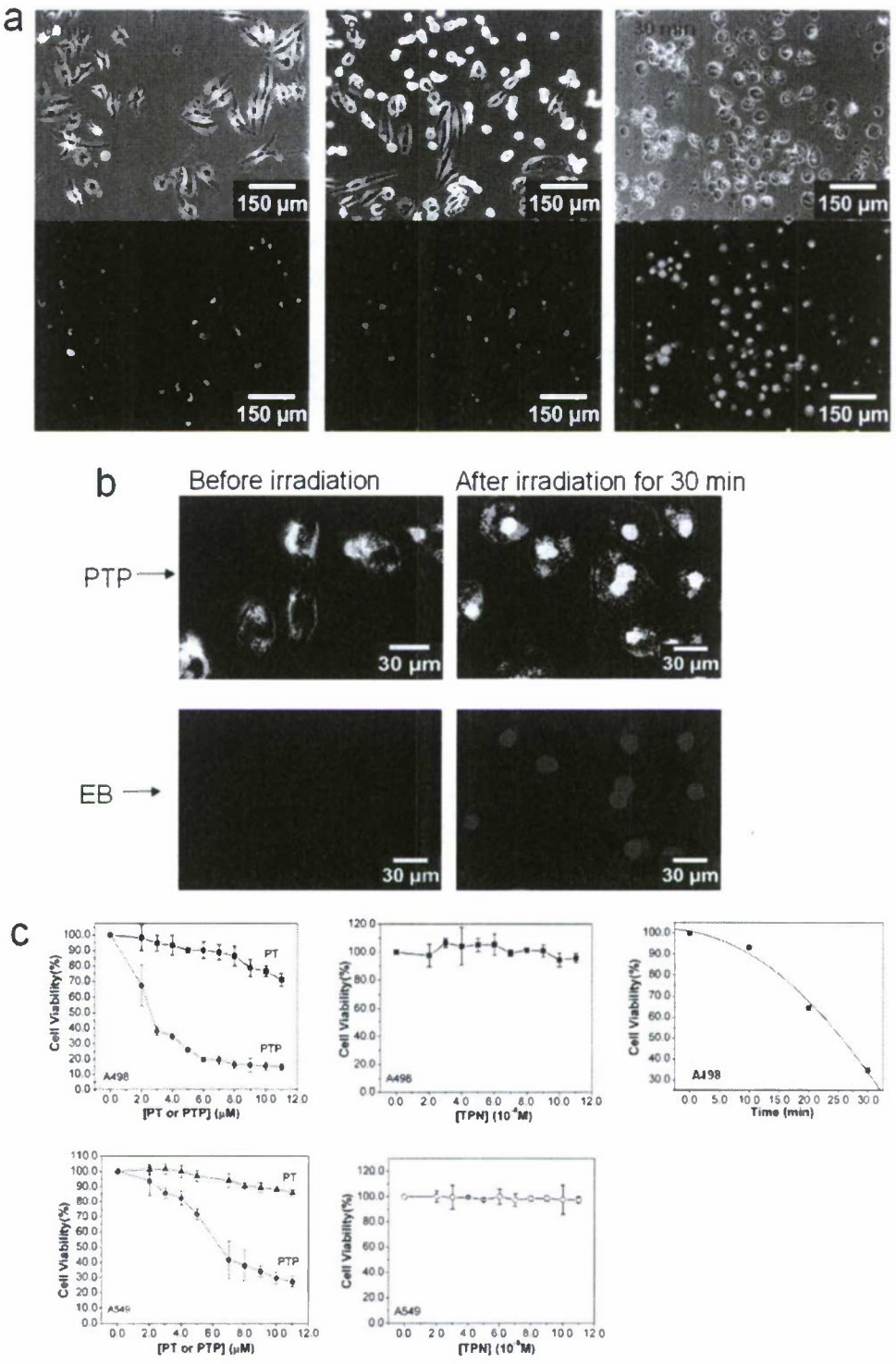

Figure 2. Apoptosis and imaging of A498 and A549 cancer cells by PTP upon irradiation at 470 nm with a 2.5 J ·cm^{-2} source. (a) Phase contrast bright-field images (upper) of A498 cells upon light irradiation from 0 to 30 min in the presence of PTP and overlapping fluorescence images of A498 cells (bottom) under PTP and EB filters. Phase contrast images were taken at

100 ms and the fluorescence images were taken at 300 ms under PTP and EB filters. The magnification of objective lens is 10×. (b) Overlapping images of A498 cancer cells under phase contrast bright field and under fluorescence field for PTP and EB before and after 30 min irradiation. The magnification of objective lens is 40×. (c) Dose-response curve data for cell viability of A498 and A549 cells treated with PTP, PT and TPN by using a typical MTT assay under 470 nm light irradiation, and the cell viability of A498 cell treated with PTP versus different durations of light exposure. Error bars correspond to standard deviations from three separate measurements.

It seemed reasonable that PTP could also find utility in antifungal therapy, based on its physical properties and observations upon interaction with cancer cells. Such a process is initiated by PTP binding to the cell envelope of fungi by electrostatic and hydrophobic interactions. Photogeneration of $^1O_2$ was anticipated to damage the outer membrane and inhibit spore germination.[31] *Aspergillus niger* (*A. niger*) was chosen for these studies since it is one of the most common species of the genus Aspergillus, is more resistant to antimicrobial agents than other species such as *Candida albicans*, and is responsible for mold infections on plants and fungal ear infections in animals and humans.[32,33] The antifungal activities of PTP, PT and TPN toward *A. niger* were first studied using a broth dilution method.[34] We evaluated the minimal inhibitory concentration (MIC) of PTP against *A. niger*. The MIC corresponds to the concentration at which no growth of *A. niger* can be observed visually. As shown in **Figure 3a**, upon white light irradiation, microplates remained clear (white color) at PTP concentration higher than 5.0 μM after 72 h incubation, whereas microplates with PT and TPN demonstrated dense confluent growth (black color) even at higher concentrations. Therefore, PT and TPN show little antifungal activities when exposed to white light, even at

concentrations as high as 15 μM, while PTP exhibits efficient antifungal activity. These results allow us to estimate the MIC of PTP to be approximately 5.0 μM.

Antifungal activities in the dark and under white light were further studied by a spectrophotometric method by varying photosensitizer concentrations. The viability fraction was determined by dividing the optical density (OD) readings of samples with photosensitizers by the OD from control readings carried out in the absence of photosensitizers. As shown in **Figure 3b**, the cell viability of *A. niger* decreases gradually with increasing PTP concentration and is down to 15% when [PTP] = 20 μM in RUs; no inhibition of cell viability for PT and TPN is observed under similar conditions. Control experiments show negligible modification of fungus viability upon treating with PTP, PT and TPN in the dark. Therefore, the efficient antifungal activity of PTP requires photoexcitation, and subsequent energy transfer from polythiophene to the porphyrin sites.

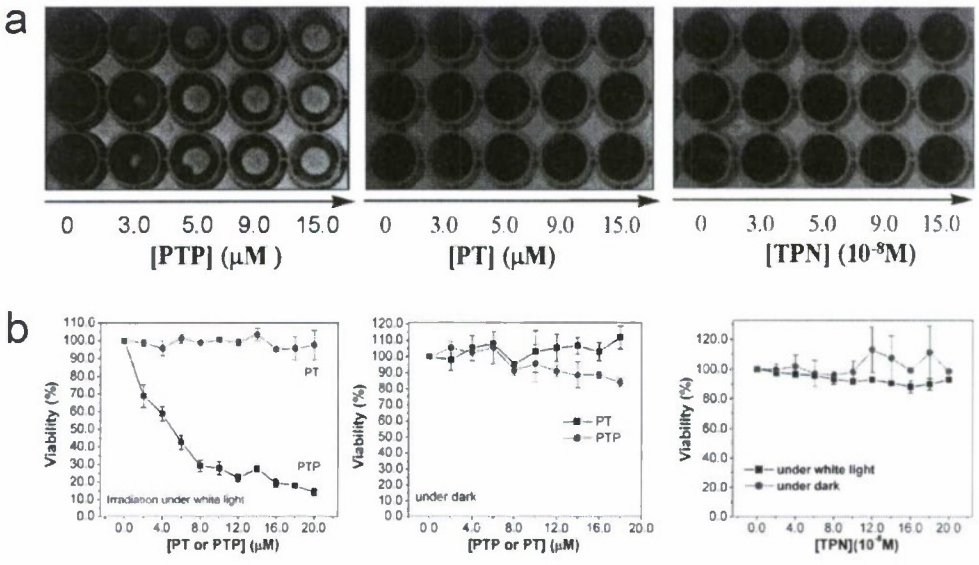

Figure 3. Antifungal activities of PTP, PT and TPN toward *A. niger* in the dark and under white light. (a) Visual images of antifungal susceptibility testing toward *A. niger* under white

light by broth dilution assay for PTP, PT and TPN with various doses. (b) The dose-response curve data for growth inhibition of *A. niger* treated with PTP, PT and TPN under white light as well as in the dark by spectrophotometric method. The white light dose was 90 J $\cdot cm^{-2}$ (irradiation for 30 min at a fluence rate of 50 mW cm^{-2}). The viability fraction was determined by dividing the optical density values of samples with photosensitizers by the values from control experiments. Error bars represent standard deviations of the data from three separate measurements.

To obtain further insight into the mechanism of antifungal activity, the interactions of PTP with the outer surface of *A. niger* were examined by fluorescence and phase contrast microscopy, as well as by scanning electron microscopy (SEM). As shown in **Figure 4a**, the fungal cell envelope emits bright fluorescence upon treatment with PTP, indicating accumulation of the conjugated polyelectrolyte on the cell surface. The SEM image of *A. niger* shows a large number of branching hypha and higher magnification SEM image indicates that the cell has a smooth outer surface (**Figure 4b**). Upon treatment with PTP, the outer cell surface becomes coarse and contains what appear to be PTP aggregates (**Figure 4c**). Because the cell envelope of *A. niger* is mainly composed of chitin, glucans, polyphosphate, and a small quantity of proteins, lipids and other biopolymers, electrostatic and hydrophobic interactions with the amphiphilic PTP lead to strong binding.[35] These conditions result in the PTP-photogenerated $^1O_2$ to be sufficiently close in proximity so that it can effectively damage the outer membrane and inhibit spore germination.

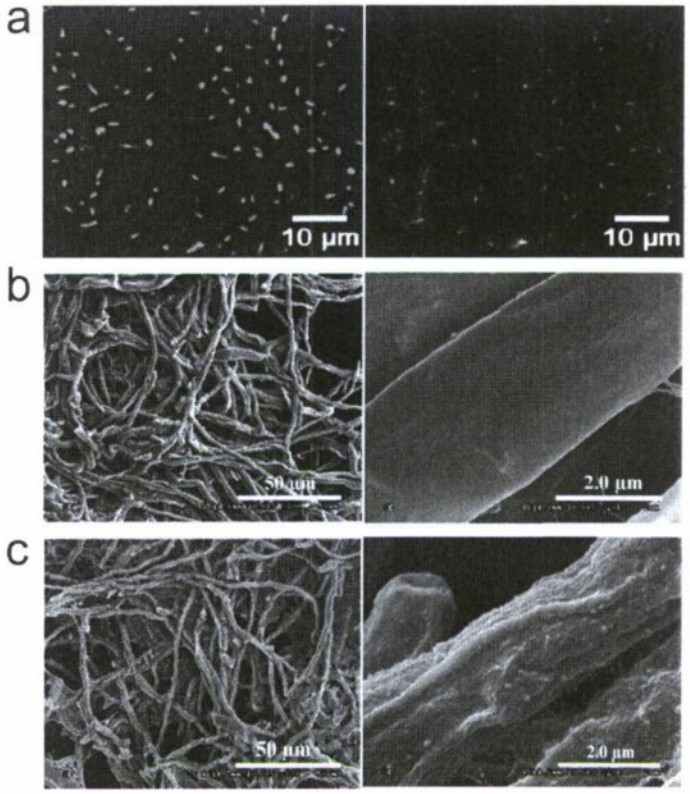

Figure 4. Binding of PTP to the outer surface of *A. niger*. (a) Phase contrast image (left) and fluorescence image (right) of *A. niger* incubated with PTP ([PTP] = 10.0 μM in RUs). The phase contrast image was taken at 100 ms exposure time and the fluorescence image was taken at 1000 ms exposure time. The magnification of objective lens is 40×. (b) Lower magnification (left) and higher magnification (right) SEM images of *A. niger* itself. (c) Lower magnification (left) and higher magnification (right) SEM images of *A. niger* coated with PTP.

In conclusion, we have designed, synthesized and characterized the therapeutic function of PTP, a novel conjugated polyelectrolyte that incorporates a cationic polythiophene backbone with pendant porphyrin chromophores. Excitation of the backbone leads to efficient, but not complete, energy transfer to the porphyrin sites, where sensitization of molecular oxygen to produce $^1O_2$ takes place. Because of the light harvesting properties of

the polymer backbone it is possible to attain higher levels of $^1O_2$ generation than when using similar concentrations of the porphyrin unit. Excitation of PTP in the presence of cancer cells leads to cell death much more efficiently than with the control polymer PT and the small molecular analogue TPN. These data demonstrate how the efficient polythiophene/porphyrin optical coupling within the conjugated polyelectrolyte structure translates into light dosages that are competitive with those of approved photosensitizers. Also noteworthy is that the residual polymer emission can be used to determine whether cancer cells are living or not, depending on the regions of highest intensities. The optical properties of PTP therefore enable treatment through $^1O_2$ generation via energy transfer, as well as monitoring of action by virtue of the residual emission. We have also shown that the $^1O_2$ formation by PTP can be used to inhibit the growth of *Aspergillus niger*, which is more resistant than other fungi, with low minimal inhibitory concentration. Importantly, PTP does not cause toxicity toward cells and fungi in the dark as a result of the low pendant porphyrin content. This collected set of observations indicates that PTP is a promising multifunctional photosensitive agent for treating cancer and fungal infections and highlights the enormous potential offered by understanding the interactions of optically active conjugated polyelectrolytes with living microorganisms.

METHODS

MATERIALS

The disodium salt of 9,10-anthracenedipropionic acid (ADPA) was prepared according to the procedure in literature.[24] The microorganism *A. niger* 3.0808 was procured from the China

General Microbiological Culture Collection Center. Ethidium bromide (EB) was purchased from Sigma. Pulmonary adenocarcinoma cell (A549) and renal cell carcinoma (A498) were purchased from cell culture center of Institute of Basic Medical Sciences, Chinese Academy of Medical Sciences (Beijing, China) and cultured in Dulbecco's Modified Eagle's Medium (DMEM) supplemented with 10% neonatal bovine serum (NBS), 4.0 mM glutamine and 4500 mg/L glucose. NBS was purchased from Sijiqing Biological Engineering Materials (Hangzhou, China). DMEM was purchased from HyClone/Thermofisher (Beijing, China). (3-(4,5-Dimethylthiazol-2-yl)-2,5-diphenyl-2H-tetrazolium hydrobromide) (MTT) was obtained from Xinjingke Biotech. (Beijing, China) and dissolved in 1×PBS before use. The water was purified using a Millipore filtration system.

MEASUREMENTS

The absorbance for MTT analysis was recorded on a microplate reader (BIO-TEK Synergy HT) at a wavelength of 520 nm. The ^{1}H NMR and ^{13}C NMR spectra were recorded on a Bruker Avance 400 MHz spectrometer. Elemental analyses were carried out with a Flash EA1112 instrument. The fluorescence spectra were measured on a Hitachi F-4500 fluorometer with a Xenon lamp as excitation source. UV-vis absorption spectra were taken on a Jasco V-550 spectrometer. Phase contrast bright-field and fluorescence images were taken on a fluorescence microscope (Olympus 1 × 71) with a mercury lamp (100 W) as light source. The excitation wavelength was 540/40 nm for EB. The morphologies of the PTP on *A. niger* were observed on a JEOL JSM 4800F field-emission scanning electron microscope, at an accelerating voltage of 15 kV. Experiments for photosensitized damage of fungi as well as tumor and normal cells were performed with a metal halogen lamp (Mejiro Genossen

MVL-210) that simulated a white light source. The wavelength was between 400 and 800 nm. The intensities of incident beams were checked by a power and energy meter and the white light dose used for irradiation was 90 J $\cdot cm^{-2}$ in the PACT toward *A. niger* and the 470nm light with a dose of 2.5 J $\cdot cm^{-2}$ obtained by the type of 470/10 nm filter was used for PDT against tumor and normal cells.

SINGLET OXYGEN MEASUREMENT

To 300 μL of the aqueous solutions of PTP, PT or TPN were added 6 μL of ADPA solution in water (6 mM). D_2O was used to replace H_2O in these experiments. The UV-vis absorption spectra were measured at 1.0 min intervals after the samples were irradiated with white light and the reduction in absorption of ADPA at 378 nm was plotted as a function of the irradiation time.

MEASUREMENT OF ANTIFUNGAL ACTIVITIES

A spore stock suspension was obtained by growing the fungus on a modified Martin agar medium slant (sterilization at 121 °C for 20 min) at 26°C for 4-5 days.[36] The conidia were harvested from the surface by adding sterile Millipore water and scraping the surface with a sterile spatula. The final spore concentration was adjusted to about 5×10^5 spores by dilution using sterilized distilled water/modified Martin broth medium (2:1). 80 μL of spore solution was placed into each well of 96-well plates and then 20μL of PTP, PT or TPN with various concentrations were added to each well. The wells containing 80 μL of spore solution and 20 μL of sterilized distilled water without photosensitizers were served as growth controls. To

test the phototoxicity of photosensitizers, the spore solutions were incubated at 26°C for 30 min in dark and then exposed to an optical fiber of 50 mW/cm^2 white light for 30min (90 J cm^{-2}). Then the plates were incubated at 26°C for another 72 h in dark and the microplates were read with a spectrophotometer at 620 nm. The viability fraction was determined by dividing the OD readings of samples with photosensitizers by the control readings that was carried out in the absence of photosensitizers. The minimum inhibitory concentration (MIC) for photosensitizers was taken at the dose where no fungal growth was observed.

CELL VIABILITY ASSAY BY MTT

A498 cells, A549 cells and fibroblast cells were routinely grown in DMEM (high glucose) medium containing 10% NBS. All cell lines were harvested for subculture using trypsin (0.05%, Gibco/Invitrogen) and grown in a humidified atmosphere containing 5% CO_2 and 95% air at 37°C. Cells were subcultured in 96-well plates the day before the experiment at a density of 4~7×10^4 cells/well, and then cultured for 24 h. PTP, PT, TPN with varying concentrations were respectively added into the cells followed by further culture for 24 h. The culture media were discarded and 100 μL of fresh cell growth medium was added. PDT treatment was performed by using he 470 nm light obtained by the type of 470/10 nm filter with a dose of 2.5J ·cm^{-2} at a fluence rate of 1.4 mW·cm^{-2} for 30 min of irradiation. The cells were allowed to continue growth for 24h, at which time the the culture media were discarded and MTT (1 mg/mL, 100 μL/well) was added to the wells followed by incubation at 37°C for 4 h. The supernatant was abandoned, and 150 μL DMSO per well was added to dissolve the produced formazan and the plates were shaken for an additional 10 min. The absorbance

values of the wells were then read with microplate reader at a wavelength of 520 nm. The cell viability rate (VR) was calculated according to the following equation where the control group was carried out in the absence of photosensitizers.

$$VR\ (\%) = \frac{A_{\text{experimental group}}}{A_{\text{control group}}}\ \text{¡Á}100\%$$

IN VITRO IMAGING OF PHOTOINDUCED DEATH OF A498 CELLS BY PTP

The A498 cells were seeded in 35 mm culture plates (Nunc) at a density of approximately 8×10^4 cells/plate for 24 h, and then the cells were washed once with 1×PBS and then grown in 1 mL DMEM medium with 10 μM PTP. After the cells were further cultured for 12 h, then the culture media were discarded and fresh DMEM medium was added. The plates were irradiated under 470 nm light for 0, 10 and 30 min respectively, then ethidium bromide (EB) was added to the samples that had been illuminated by light, and they were then observed by fluorescence microscopy. Upon addition of EB to the samples, the phase contrast images were taken at 100 ms and the fluorescence images were taken at 300 ms under PTP and under EB filters. The false color of PTP is yellow and the type of light filter is D455/70 nm exciter, 500 nm beamsplitter, and D600/50 nm emitter. The false color of EB is red and the type of light filter is D540/40 nm exciter, 570 nm beamsplitter, and D600/50 nm emitter.

Acknowledgments

The authors are grateful for the National Natural Science Foundation of China (No. 20725308, 90913014 and TRR61), the Major Research Plan of China (No. 2006CB932100), the National Science Foundation ((DMR 0606414), the ITC-PAC (Contract No. FA5209-08-P-0365) and

the Institute for Collaborative Biotechnologies at the University of California, Santa Barbara.

Author contributions

C. X., L. L. and S.W. designed experiments, analysed data and organized the manuscript. H. T., X. F. and Q. Y analysed data. G. C. B. analysed data and organized the manuscript.

Additional information

The authors declare that they have no competing financial interests. Supplementary Information accompanies this paper on www.nature.com/naturematerials.

References.

1. Swager, T. M. The Molecular Wire Approach to Sensory Signal Amplification. *Acc. Chem. Res.* **31**, 201-207 (1998).
2. Liu, B. & Bazan, G. C. Homogeneous fluorescence-based DNA detection with water-soluble conjugated polymers. *Chem. Mater.* **16**, 4467-4476 (2004).
3. Lakowicz, J. R. *Principles of Fluorescence Spectroscopy* (Kluwer Academic/Plenum, 1999).
4. Thomas, S.W. III, Joly, G. D., Swager, T. M. Chemical sensors based on amplifying fluorescent conjugated polymers. *Chem. Rev.* **107**, 1339-1386 (2007).
5. Ho, H. A., Najari, A. & Leclerc, M. Optical detection of DNA and proteins with cationic polythiophenes, *Acc. Chem. Res.* **41**, 168-178 (2008).
6. Duan, X., Liu, L., Feng, F., Wang, S. Cationic conjugated polymers for optical detection of DNA methylation, lesions, and single nucleotide polymorphisms. *Acc. Chem. Res.* **43**,

260-270 (2010).

7. Bunz, U. H. F., Rotello, V. M. Gold nanoparticle-fluorophore complexes: sensitive and discerning "noses" for biosystems sensing. *Angew. Chem. Int. Ed.* **49**, DOI: 10.1002/anie.200906928 (2010).

8. Achyuthan, K. E. et al. Fluorescence superquenching of conjugated polyelectrolytes: applications for biosensing and drug discovery. *J. Mater. Chem.* **15**, 2648-2656 (2005).

9. Jiang, H., Taranekar, P., Reynolds, J. R., Schanze, K. S. Conjugated polyelectrolytes: synthesis, photophysics, and applications. *Angew. Chem. Int. Ed.* **48**, 4300-4316 (2009).

10. Wu, C., Bull, B., Christensen, K., McNeill, J. Ratiometric single-nanoparticle oxygen sensors for biological imaging. *Angew. Chem. Int. Ed.* **48**, 2741-2745 (2009).

11. Wu, C. L. & Xu, Q. H. Enhanced one- and two-photon excitation emission of a porphyrin photosensitizes by FRET from a conjugated polyelectrolyte. *Macromol. Rapid Commun.* **30**, 504-508 (2009).

12. Oar, M. A. et al. Light-harvesting chromophores with metalated porphyrin cores for tuned photosensitization of singlet oxygen via two-photon excited FRET. *Chem. Mater.* **18**, 3682-3692 (2006).

13. Chen, C.-Y. et al. Two-photon absorbing block copolymer as a nanocarrier for porphyrin: energy transfer and singlet oxygen generation in micellar aqueous solution. *J. Am. Chem. Soc.* **129**, 7220-7221 (2007).

14. Xing, C., Xu, Q., Tang, H., Liu, L., Wang, S. Conjugated polymer/porphyrin complexes for efficient energy transfer and improving light-activated antibacterial activity. *J. Am. Chem. Soc.* **131**, 13117-13124 (2009).

15. Celli, J. P. et al. Imaging and photodynamic therapy: mechanisms, monitoring, and optimization. *Chem. Rev.* **110**, DOI: 10.1021/cr900300p (2010).

16. Dolmans, D. E., Fukumura, D., Jain, R. K. Photodynamic therapy for cancer. *Nat. Rev. Cancer* **3**, 380-387 (2003).

17. Cowen, L. E. The evolution of fungal drug resistance: modulating the trajectory from genotype to phenotype. *Nat. Rev. Microbiol.* **6**, 187-198 (2008).

18. Mitoraj, D. et al. Visible light inactivation of bacteria and fungi by modified titanium dioxide. *Photochem. Photobiol. Sci.* **6**, 642–648 (2007).

19. Tegos, G. P. et al. Protease-stable polycationic photosensitizer conjugates between polyethyleneimine and chlorin(e6) for broad-spectrum antimicrobial photoinactivation. *Antimicrob. Agents. Chemother.* **50**, 1402-1410 (2006).

20. Demidova, T. N. & Hamblin, M. R. Effect of cell-photosensitizer binding and cell density on microbial photoinactivation. *Antimicrob. Agents. Chemother.* **49**, 2329–2335 (2005).

21. Kim, O.-K., Je, J. & Melinger, J. S. One-dimensional energy/electron transfer through a helical channel. *J. Am. Chem. Soc.* **128**, 4532-4533 (2006).

22. Wu, C., Bull, B., Szymanski, C., Christensen, K. & McNeill, J. Multicolor conjugated polymer dots for biological fluorescence imaging. *ACS Nano*. **2**, 2415-2423 (2008).

23. Feng, X., Tang, Y., Duan, X., Liu, L. & Wang, S. Lipid-modified conjugated polymer nanoparticles for cell imaging and transfection. *J. Mater. Chem.* **20**, 1312-1316 (2010).

24. Lindig, B. A., Rodgers, M. A. J. & Schaap, A. P. Determination of the lifetime of singlet oxygen in water-d2 using 9,10-anthracenedipropionic acid, a water-soluble probe. *J. Am. Chem. Soc.* **102**, 5590-5593 (1980).

25. Buytaert, E.; Dewaele, M. & Agostinis, P. Molecular effectors of multiple cell death pathways initiated by photodynamic therapy. *Biochim. Biophys. Acta.* **1776,** 86–107 (2007).

26. Nicholson, D. W. From bench to clinic with apoptosis-based therapeutic agents. *Nature* **407**, 810-816 (2000).

27. Darzynkiewicz, Z. Cytometry in cell necrobiology: analysis of apoptosis and accidental cell death (necrosis). *Cytometry* **27**, 1-20 (1997).

28. Denizot, F. & Lang, R. Rapid colorimetric assay for cell growth and survival. *J. Immunol. Methods* **89**, 271-277 (1986).

29. Jendželovskỳ, R. *et al.* Drug efflux transporters, MRP1 and BCRP, affect the outcome of hypericin-mediated photodynamic therapy in HT-29 adenocarcinoma cells. *Photochem. Photobiol. Sci.* **8**, 1716-1723 (2009).

30. Ris, H. B. *et al.* Photodynamic therapy with chlorins for diffuse malignant mesothelioma: initial clinical results. *Br. J. Cancer* **64**, 1116–1120 (1991).

31. Bertoloni, G., Zambotto, F., Conventi, L., Reddi, E. & Jori, G. Role of specific cellulartargets in the hematoporphyrin-sensitized photoinactivation of microbialcells. *Photochem. Photobiol.* **46**, 695–698 (1987).

32. Pitt, J. I. & Hocking, A. D. *Fungi and food spoilage,* 2nd ed.; Blackie Academic and Professional: London, U.K., 1997.

33. Varga, J.; Juhasz, A.; Kevei, F. & Kozakiewicz, Z. Molecular diversity of agriculturally important *Aspergillus* species. *Eur. J. Plant Pathol.* **110**, 627–640 (2004).

34. Llop, C., Pujol, I., Aguilar, C., Sala, J., Riba, D. & Guarro. J. Comparison of three

methods of determining MICs for filamentous fungi using different end point criteria and incubation periods. *Antimicrob. Agents. Chemother.* **44**, 239–242 (2000).

35. Liu, L., Duan, X., Liu, H., Wang, S. & Li, Y. Microorganism-based assemblies of luminescent conjugated polyelectrolytes. *Chem. Commun.* 5999–6001(2008).
36. Bapat, P. M.; Kundu, S. & Wangikar, P. P. An optimized method for Aspergillus niger spore production on natural carrier substrates. *Biotechnol. Prog.* **19**, 1683-1688 (2003).